Time-domain multi-patch discontinuous Galerkin methods

Jesse Chan[1], J. A. Evans[2]

[1]Department of Computational and Applied Math, Rice University
[2]Ann and H.J. Smead Aerospace Engineering Sciences, UC Boulder

USNCCM 2017
July 18, 2017

High order Galerkin methods for hyperbolic PDEs

- Time-dependent solutions of hyperbolic equations.
- Low numerical dissipation and dispersion.
- High order approximations: more accurate per unknown.
- High performance on many-core (explicit time-stepping).

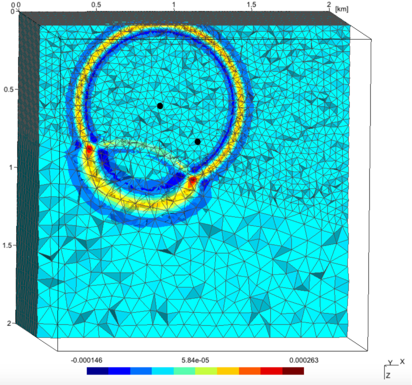

Figure courtesy of Axel Modave.

High order Galerkin methods for hyperbolic PDEs

- Time-dependent solutions of hyperbolic equations.
- Low numerical dissipation and dispersion.
- High order approximations: more accurate per unknown.
- High performance on many-core (explicit time-stepping).

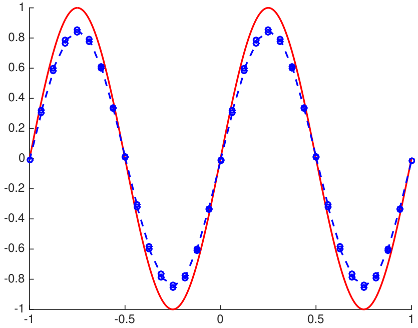

Fine linear approximation.

High order Galerkin methods for hyperbolic PDEs

- Time-dependent solutions of hyperbolic equations.
- Low numerical dissipation and dispersion.
- High order approximations: more accurate per unknown.
- High performance on many-core (explicit time-stepping).

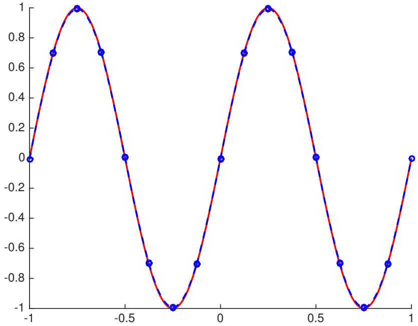

Coarse quadratic approximation.

High order Galerkin methods for hyperbolic PDEs

- Time-dependent solutions of hyperbolic equations.
- Low numerical dissipation and dispersion.
- High order approximations: more accurate per unknown.
- High performance on many-core (explicit time-stepping).

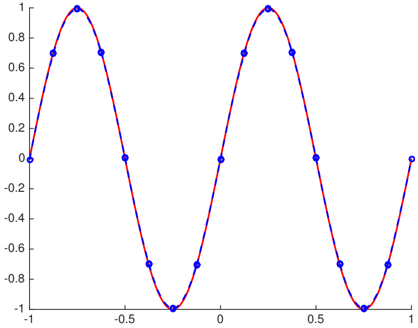

Coarse quadratic approximation.

High order Galerkin methods for hyperbolic PDEs

- Time-dependent solutions of hyperbolic equations.
- Low numerical dissipation and dispersion.
- High order approximations: more accurate per unknown.
- High performance on many-core (explicit time-stepping).

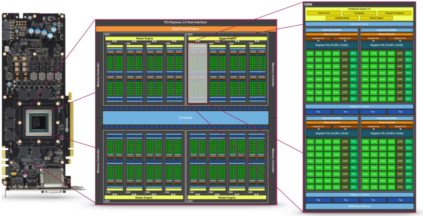

A graphics processing unit (GPU).

Multi-patch discontinuous Galerkin formulations

- Model problem: (second order) acoustic wave equation

$$\frac{1}{c^2}\frac{\partial^2 p}{\partial t^2} - \Delta p = f.$$

- Pressure-velocity system (first order formulation)

$$\frac{1}{c^2}\frac{\partial p}{\partial t} + \nabla \cdot \boldsymbol{u} = f$$
$$\frac{\partial \boldsymbol{u}}{\partial t} + \nabla p = 0.$$

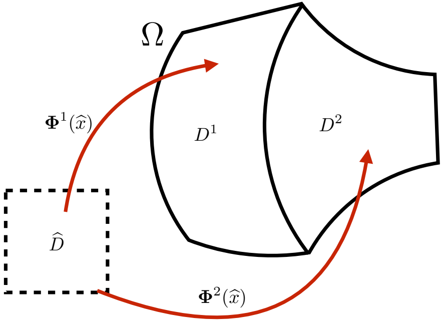

- Weak patch coupling through DG numerical flux (SIPG, upwind).

Langer et al 2014. Multipatch discontinuous Galerkin isogeometric analysis.

Wilcox et al 2010. A high-order DG method for wave propagation through coupled elastic-acoustic media.

Method of lines multi-patch DG discretization

- Semi-discrete system:

$$\boldsymbol{M}_h \frac{\mathrm{d}\boldsymbol{u}}{\mathrm{d}t} = \boldsymbol{A}_h \boldsymbol{u} \quad \Rightarrow \quad \frac{\mathrm{d}\boldsymbol{u}}{\mathrm{d}t} = \boldsymbol{M}_h^{-1} \boldsymbol{A}_h \boldsymbol{u}.$$

- Global mass matrix $\boldsymbol{M}_h$ is (patch) block diagonal.
- Tailored patch discretizations: explicit time-stepping, curved domains.
    - Efficient mass matrix inversion over each patch.
    - High order accuracy, energy stability on curved geometries.
    - Improved stable timestep restriction (CFL).

Outline

Outline

B-spline basics

- Standard 1D B-splines: $B_i^0(x) = \mathbb{1}_{\xi_i \leq x \leq \xi_{i+1}}$,

$$B_i^k(x) = \frac{x - \xi_i}{\xi_{i+p} - \xi_i} B_i^{k-1}(x) + \frac{\xi_{i+p+1} - x}{\xi_{i+p+1} - \xi_{i+1}} B_{i+1}^{k-1}(x).$$

- Assume patches are mapped quads/cubes: tensor product basis

$$B_{ijk}^p(x, y, z) = B_i^p(x) B_j^p(y) B_k^p(z).$$

- Assume maximally continuous, open knot vectors

$$\xi_{p+1} < \ldots < \xi_{p+1+K},$$
$$\xi_1 = \ldots = \xi_{p+1},$$
$$\xi_{p+1+K} = \ldots = \xi_{2p+1+K}.$$

B-spline bases and optimal spline spaces

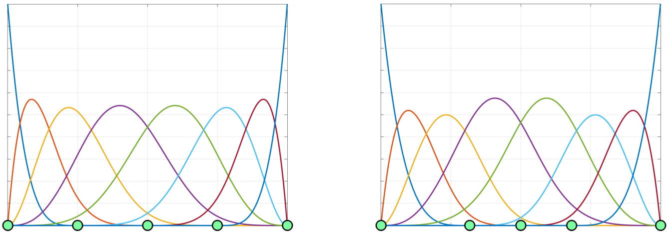

(a) Uniform knots (b) Optimal knots

- Sup-inf: "worst best approximation" in X from X_n

$$d_n(X; X_n) = \sup_{x \in X} \inf_{y \in X_n} \|x - y\|, \qquad \dim(X_n) = n.$$

- Spline spaces with optimal knot vectors: minimal sup-inf for

$$X = \left\{ f \in L^2([-1,1]) : \frac{\partial^{p-1} f}{\partial x^{p-1}} \text{ continuous}, \quad \|f\|_{L^2} \leq 1 \right\},$$

Melkman and Micchelli 1978. Spline spaces are optimal for L^2 n-width.

Optimal knot vectors: roots of eigenfunctions

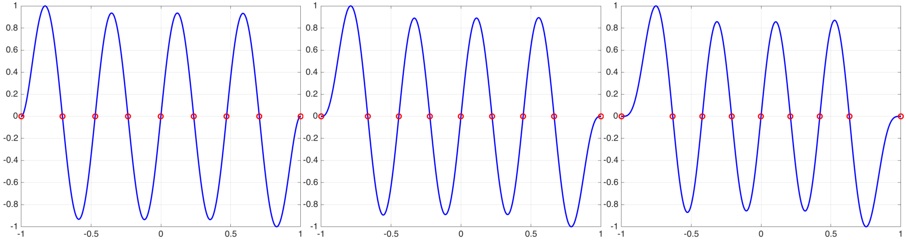

(a) $p = 2$ (b) $p = 3$ (c) $p = 4$

Figure: Eigenfunctions $y_{K+1,p}(x)$ for $K = 8$ and various p.

- Optimal knots are roots of eigenfunctions $y_{K+1,p}(x)$.

$$(-1)^p \frac{\partial^{2p} y}{\partial x^{2p}} = \lambda y(x), \qquad \frac{\partial^k y}{\partial x^k}(-1) = \frac{\partial^k y}{\partial x^k}(1) = 0, \quad 1 \leq k \leq p-1.$$

- Approximate $y_{K+1,p}(x)$ using fine spline space; difficult for high K, p!

Knot smoothing: approximating optimal knots

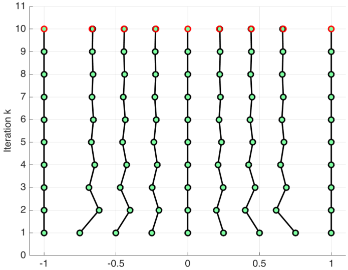

(a) Knots ξ_i (optimal in red)

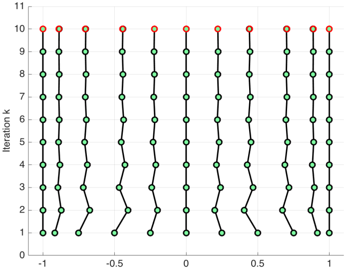

(b) Greville abscissae τ_j

- Greville abscissae τ_j: coefficients for linear coordinate x.

$$x = \sum_{1 \leq j \leq p+K} \tau_j B_j^p(x), \qquad \tau_j = \frac{1}{p} \sum_{1 \leq i \leq p} \xi_{i+j-1}, \quad j = 1, \ldots, p.$$

- Replace Greville abscissae with equispaced points $\widehat{x}_i$ and iterate

$$\tilde{\xi}_i^{k+1} = \sum_{1 \leq j \leq p+K} \widehat{x}_i B_j^p(\xi_i; \tilde{\xi}^k), \qquad \tilde{\xi}_i^0 = \xi_i,$$

Knot smoothing: approximating optimal knots

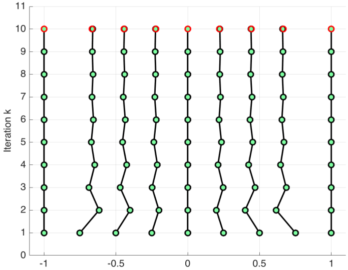

(a) Knots ξ_i (optimal in red)

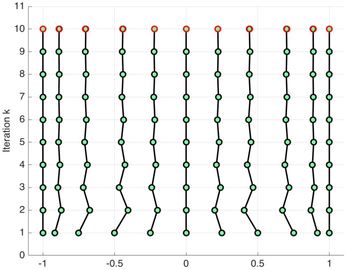

(b) Greville abscissae τ_j

- Greville abscissae τ_j: coefficients for linear coordinate x.

$$\xi_i = \sum_{1\leq j\leq p+K} \tau_j B_j^p(\xi_i), \qquad \tau_j = \frac{1}{p}\sum_{1\leq i\leq p} \xi_{i+j-1}, \quad j = 1,\ldots,p.$$

- Replace Greville abscissae with equispaced points $\widehat{x}_i$ and iterate

$$\tilde{\xi}_i^{k+1} = \sum_{1\leq j\leq p+K} \widehat{x}_i B_j^p(\xi_i;\tilde{\xi}^k), \qquad \tilde{\xi}_i^0 = \xi_i,$$

Knot smoothing: approximating optimal knots

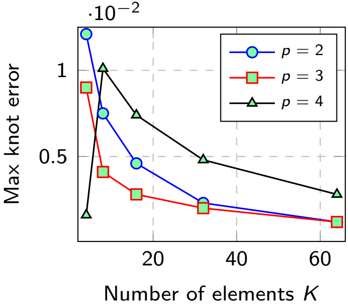

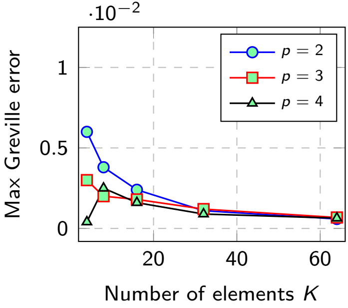

- Greville abscissae τ_j: coefficients for linear coordinate x.

$$\xi_i = \sum_{1 \le j \le p+K} \tau_j B_j^p(\xi_i), \qquad \tau_j = \frac{1}{p} \sum_{1 \le i \le p} \xi_{i+j-1}, \quad j = 1, \ldots, p.$$

- Replace Greville abscissae with equispaced points $\widehat{x}_i$ and iterate

$$\tilde{\xi}_i^{k+1} = \sum_{1 \le j \le p+K} \widehat{x}_i B_j^p(\xi_i; \tilde{\xi}^k), \qquad \tilde{\xi}_i^0 = \xi_i,$$

Approximation properties: oscillatory functions

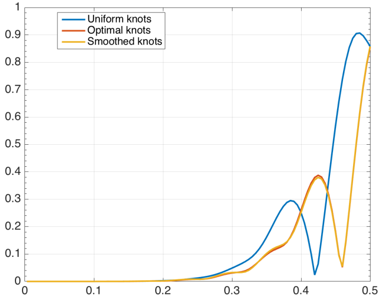

(a) L^2 error vs $k/N_{\rm dofs}$ $\left(\cos\left(\frac{k\pi x}{2}\right)\right)$

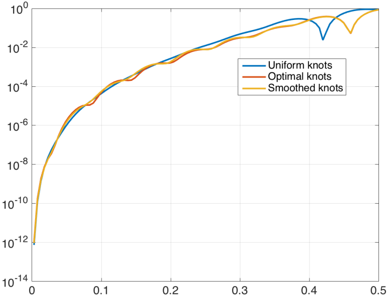

(b) Semi-log scale

- L^2 best approximations with smoothed knots (fixed p, K): decreased high frequency errors, increased low frequency errors.
- Similar errors approximating solution $\cos\left(\frac{k\pi x}{2}\right)\cos\left(\frac{k\pi t}{2}\right)$ (k odd).

Approximation properties: oscillatory functions

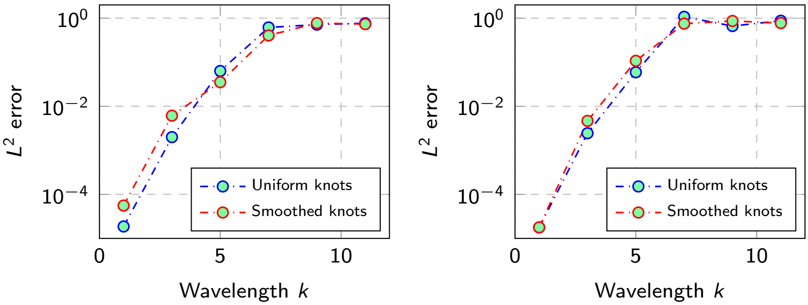

(a) First order formulation

(b) Second order formulation

- L^2 best approximations with smoothed knots (fixed p, K): decreased high frequency errors, increased low frequency errors.
- Similar errors approximating solution $\cos\left(\frac{k\pi x}{2}\right)\cos\left(\frac{k\pi t}{2}\right)$ (k odd).

Spectral properties of $\boldsymbol{A}_h$

Eigenvalues, eigenfunctions of 1D Laplacian: uniform vs smoothed knots.

$$|\lambda_k - \lambda_{h,k}|, \qquad \|w_k(x) - w_{h,k}(x)\|^2_{L^2}$$

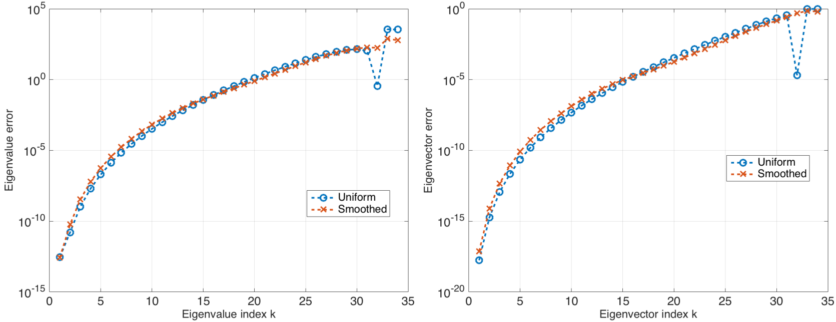

(a) Eigenvalue errors   (b) Eigenvector errors

Figure: Eigenvalue and eigenvector errors for $p = 4$, $K = 32$ splines.

Spectral properties of $\boldsymbol{A}_h$

Constant 1D advection: numerical dispersion error $|\mathrm{Re}(\omega) - \mathrm{Re}(\omega_h)|$

$$\frac{\partial u}{\partial t} + \frac{\partial u}{\partial x} = 0, \qquad u(x,t) = e^{i(kx - \omega t)}, \quad u_h(x,t) = e^{i(kx - \omega_h t)}.$$

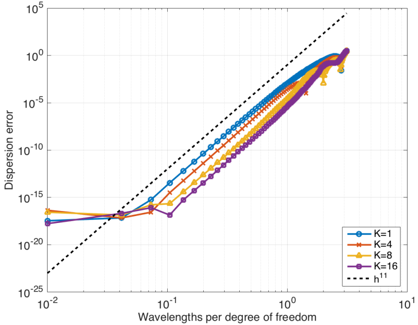

(a) Dispersion errors (uniform knots)

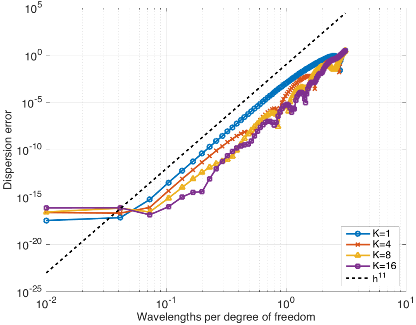

(b) Dispersion errors (smoothed knots)

Figure: Dispersion errors using full upwinding, $p = 4$, and $K = 1, 4, 8$.

Approximation properties: curvilinear domains

- Smoothed knot vectors: more accurate on curved domains.
- Differences between first, second order forms (L^2 vs energy norm?).

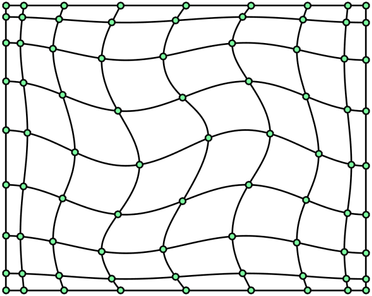

(a) Warped mesh, $\alpha = 1/8$

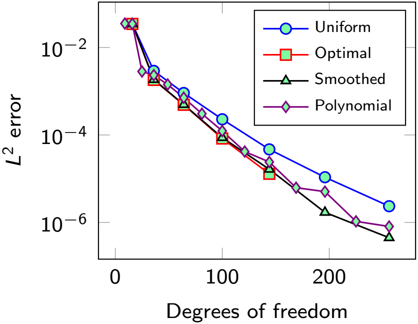

(b) L^2 errors ($\alpha = 1/64$)

Figure: L^2 approx. errors: $\cos\left(\frac{\pi x}{2}\right)\cos\left(\frac{\pi y}{2}\right)$, $p = 2, \ldots, 8$ and $K = p$.

Approximation properties: curvilinear domains

- Smoothed knot vectors: more accurate on curved domains.
- Differences between first, second order forms (L^2 vs energy norm?).

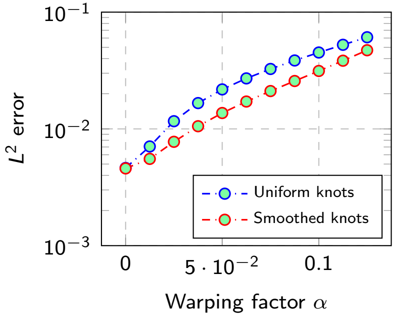

(a) First order formulation

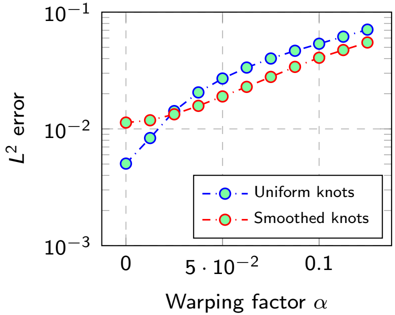

(b) Second order formulation

Figure: L^2 errors for increasing α ($p = 3, K = 8$ splines on a single patch).

Approximate mass matrix inversion

- Patch mass matrices $\boldsymbol{M}_J$: tensor product basis but no Kronecker structure due to $J(\widehat{\boldsymbol{x}})$, and mass lumping is inaccurate.

$$(\boldsymbol{M}_J)_{ijk,lmn} = \int_{\widehat{D}} B^p_{ijk}(\widehat{\boldsymbol{x}}) B^p_{lmn}(\widehat{\boldsymbol{x}}) J(\widehat{\boldsymbol{x}})\, \mathrm{d}\widehat{\boldsymbol{x}}.$$

- Preconditioning: approximating $\boldsymbol{M}_J^{-1}$ impacts semi-discrete stability. Note - Krylov methods approximate $\boldsymbol{M}_J^{-1}$ as a non-linear operator!

$$\frac{1}{2}\frac{\mathrm{d}}{\mathrm{d}t}\|u\|^2_{L^2} = \boldsymbol{u}^T \boldsymbol{M}_J \frac{\mathrm{d}\boldsymbol{u}}{\mathrm{d}t} \leq 0.$$

- Isogeometric collocation: restores tensor product structure, but semi-discrete stability is more difficult to prove.

Gao and Calo 2014. Fast isogeometric solvers for explicit dynamics.

Wathen and Rees 2009. Chebyshev semi-iteration in preconditioning for problems including the mass matrix.

Auricchio et al 2012. Isogeometric collocation for elastostatics and explicit dynamics.

Restoring Kronecker structure to $\boldsymbol{M}^{-1}$

- Replace $\boldsymbol{M}_J$ with "weight-adjusted" approximation:

$$\frac{\mathrm{d}}{\mathrm{d}t}\boldsymbol{M}_J\boldsymbol{u} \Rightarrow \frac{\mathrm{d}}{\mathrm{d}t}\widehat{\boldsymbol{M}}\boldsymbol{M}_{1/J}^{-1}\widehat{\boldsymbol{M}}\boldsymbol{u}, \qquad \left(\widehat{\boldsymbol{M}}\right)_{ijk,lmn} = \int_{\widehat{D}} B^p_{ijk}(\widehat{\boldsymbol{x}})B^p_{lmn}(\widehat{\boldsymbol{x}})\,\mathrm{d}\widehat{\boldsymbol{x}}.$$

- Weight-adjusted inverse: tensor product + matrix-free eval. of $\boldsymbol{M}_{1/J}$

$$\boldsymbol{M}_J^{-1} \approx \left(\widehat{\boldsymbol{M}}\boldsymbol{M}_{1/J}^{-1}\widehat{\boldsymbol{M}}\right)^{-1} = \widehat{\boldsymbol{M}}^{-1}\boldsymbol{M}_{1/J}\widehat{\boldsymbol{M}}^{-1}$$
$$\widehat{\boldsymbol{M}}^{-1} = \widehat{\boldsymbol{M}}_{\mathrm{1D}}^{-1} \otimes \widehat{\boldsymbol{M}}_{\mathrm{1D}}^{-1} \otimes \widehat{\boldsymbol{M}}_{\mathrm{1D}}^{-1}.$$

- Energy stability with respect to equivalent norm

$$C_1(J)\left\|\boldsymbol{u}\right\|_{\widehat{\boldsymbol{M}}\boldsymbol{M}_{1/J}^{-1}\widehat{\boldsymbol{M}}} \leq \left\|\boldsymbol{u}\right\|_{\boldsymbol{M}_J} \leq C_2\left\|\boldsymbol{u}\right\|_{\widehat{\boldsymbol{M}}\boldsymbol{M}_{1/J}^{-1}\widehat{\boldsymbol{M}}}.$$

Chan, et al. 2016. Weight-adjusted DG methods: wave prop. in heterogeneous media. (SISC).

Chan, et al. 2016. Weight-adjusted DG methods: curvilinear meshes (arXiv).

Also applied to GD methods (Banks and Hagstrom 2016. On Galerkin difference methods).

Weight-adjusted DG for curvilinear meshes

- Weight-adjusted projection $\tilde{P}_h$ on curved domains

$$\tilde{P}_h(u) := \widehat{P}_h\left(\frac{1}{J}\widehat{P}_h(uJ)\right).$$

where $\widehat{P}_h$ is the L^2 projection onto the reference element.

- L^2 estimates for weight-adjusted projection:

$$\left\|u - \tilde{P}_h u\right\|_{L^2(D^k)} \lesssim \left\|\frac{1}{\sqrt{J}}\right\|^2_{L^\infty} \|J\|_{W^{N+1,\infty}(D^k)} h^{N+1} \|u\|_{W^{N+1,2}(D^k)}.$$

High order Sobelev norm of J - can lose accuracy if the geometric mapping is not sufficiently regular!

L^2 vs weight-adjusted projection

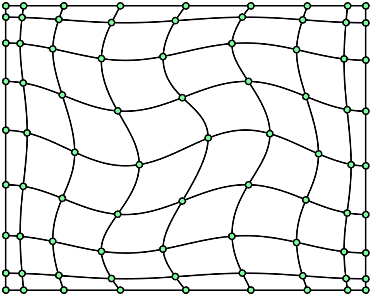

(a) Warped mesh, $\alpha = 1/8$

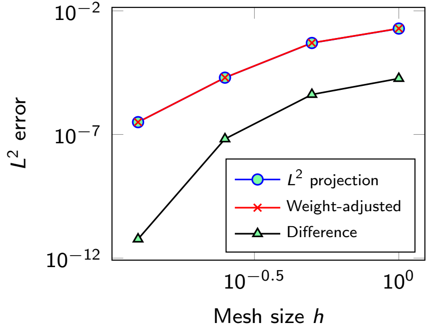

(b) L^2 errors

Figure: L^2 vs weight-adjusted projection: $\cos\left(\frac{\pi x}{2}\right)\cos\left(\frac{\pi y}{2}\right)$, $p = 4$.

Stable timestep restrictions: h, p scaling

- Estimate $dt \leq 1/\rho(\boldsymbol{M}_h^{-1}\boldsymbol{A}_h)$. Bound $\rho(\boldsymbol{M}_h^{-1}\boldsymbol{A}_h)$ using Rayleigh quotients and Bendixon-Hirsch; depends on h and **constants** C_T, C_I.

$$\|u\|_{L^2(\partial \widehat{D})} \leq C_T \|u\|_{L^2(\widehat{D})}, \qquad \|\nabla u\|_{L^2(\widehat{D})} \leq C_I \|u\|_{L^2(\widehat{D})}.$$

- CFL: $O(h/p^2)$ for polynomials, $O(h/p)$ for splines if $h \leq O(1/p)$.

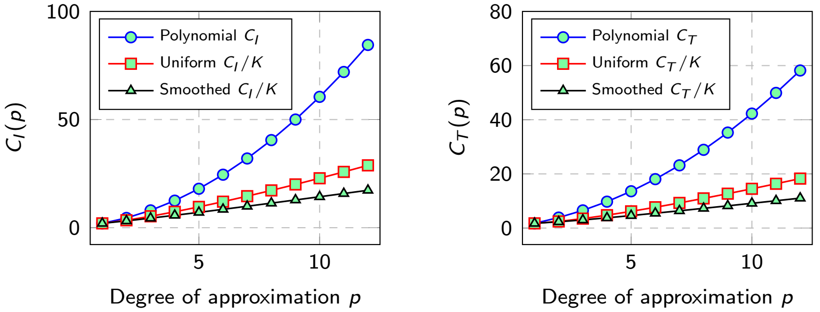

(a) Inverse inequality, $K = 2p$ (b) Trace inequality, $K = 2p$

Stable timestep restrictions: h, p scaling

- Estimate $dt \leq 1/\rho(\boldsymbol{M}_h^{-1}\boldsymbol{A}_h)$. Bound $\rho(\boldsymbol{M}_h^{-1}\boldsymbol{A}_h)$ using Rayleigh quotients and Bendixon-Hirsch; depends on h and **constants** C_T, C_I.

$$\|u\|_{L^2(\partial\widehat{D})} \leq C_T \|u\|_{L^2(\widehat{D})}, \qquad \|\nabla u\|_{L^2(\widehat{D})} \leq C_I \|u\|_{L^2(\widehat{D})}.$$

- CFL: $O(h/p^2)$ for polynomials, $O(h/p)$ for splines if $h \leq O(1/p)$.

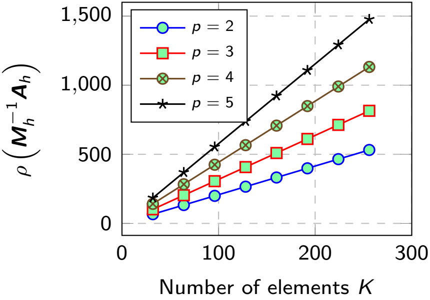

(a) Uniform knots

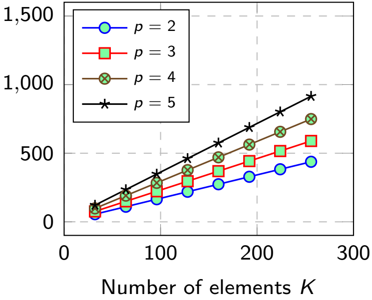

(b) Smoothed knots

A 3D multi-patch example

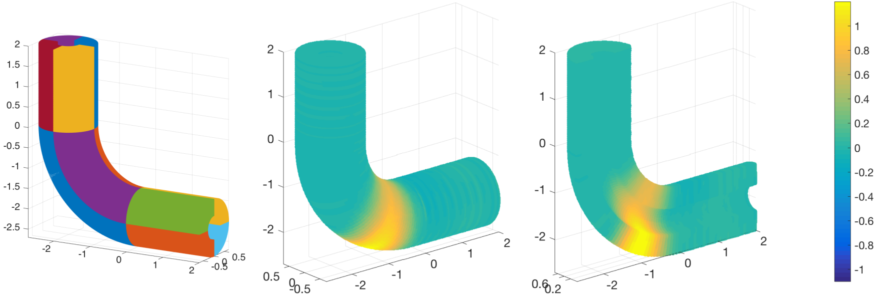

- 12 patch pipe model, first order formulation, pulse inflow condition.
- Isotropic $p = 6, K = 16$ splines, smoothed knots on each patch.

Chan, Evans. 2017. Multi-patch discontinuous Galerkin spline FEM for time-domain wave propagation (in preparation).

Summary and acknowledgements

- Optimal/smoothed knot vectors for time-domain simulations.
- Restore Kronecker product with weight-adjusted mass matrix.
- Future directions:
  - Conforming spaces for first order formulations.
  - Nonlinear systems (compressible flow).

This research is supported by DMS-1712639 and TOTAL E&P Research and Technology USA.

Chan, Evans. 2017. Multi-patch discontinuous Galerkin spline FEM for time-domain wave propagation (in preparation).

Chan, et al. 2016. Weight-adjusted DG methods: curvilinear meshes (arXiv).

Additional slides

Patch refinement vs knot insertion (uniform knots)

- Patch size H, number of sub-elements K: $h = H/K$.
- Optimal $O(h^{p+1})$ L^2 error for both patch refinement, knot insertion.

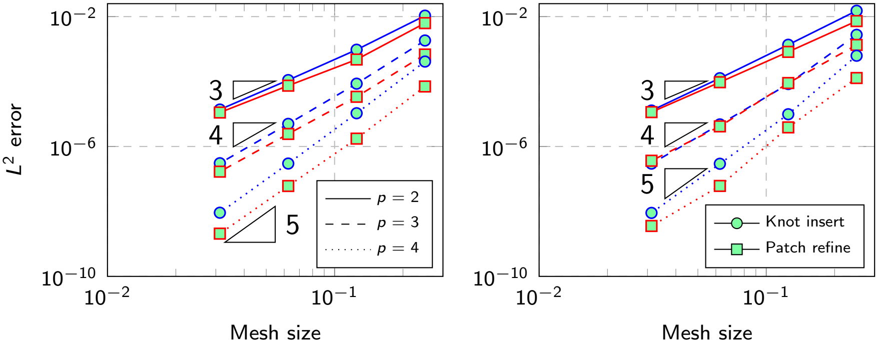

(a) First order (uniform knots)

(b) Second order (uniform knots)

Convergence of WADG on curvilinear meshes

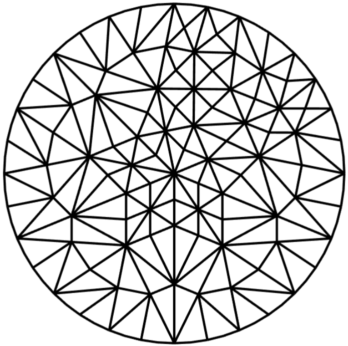

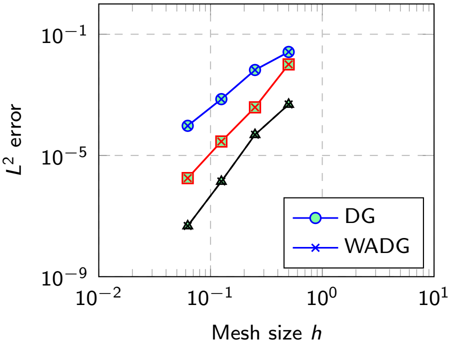

(a) L^2 errors for $N = 2, 3, 4$

Figure: Optimal L^2 convergence rates observed for curvilinear meshes.

Curvilinear meshes: DG eigenvalues (circular domain)

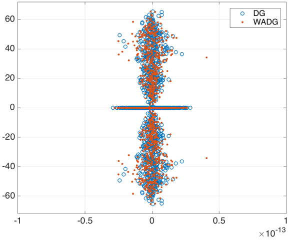

(a) Central fluxes

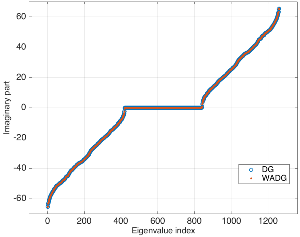

(b) $\mathrm{Im}(\lambda_i)$ for central fluxes

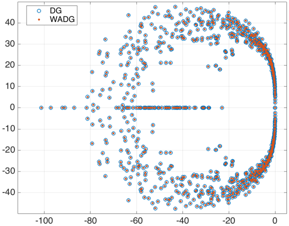

(c) Upwind fluxes

Behavior of weight-adjusted L^2 projection

Comparison with L^2 projection and Low-Storage Curvilinear DG

$$\tilde{\phi}_i = \frac{\phi_i}{\sqrt{J}}, \qquad \boldsymbol{M}_{ij} = \int_{D^k} \tilde{\phi}_j \tilde{\phi}_i J = \int_{\widehat{D}} \phi_j \phi_i = \widehat{\boldsymbol{M}}_{ij}.$$

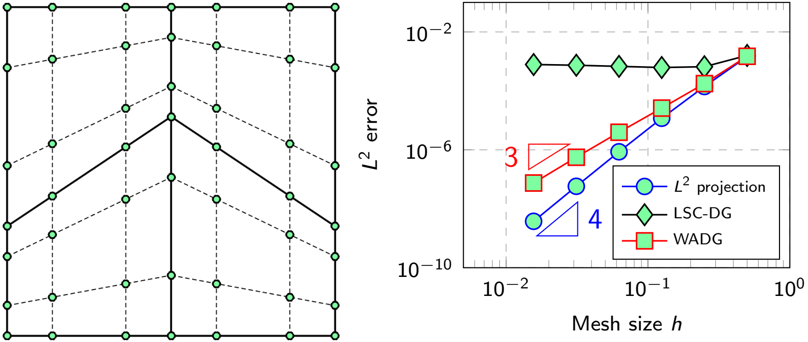

Figure: Arnold-type mesh with $\|J\|_{W^{N+1,\infty}} = O(h^{-1})$ for $N = 3$.

Behavior of weight-adjusted L^2 projection

Comparison with L^2 projection and Low-Storage Curvilinear DG

$$\tilde{\phi}_i = \frac{\phi_i}{\sqrt{J}}, \qquad \boldsymbol{M}_{ij} = \int_{D^k} \tilde{\phi}_j \tilde{\phi}_i J = \int_{\widehat{D}} \phi_j \phi_i = \widehat{\boldsymbol{M}}_{ij}.$$

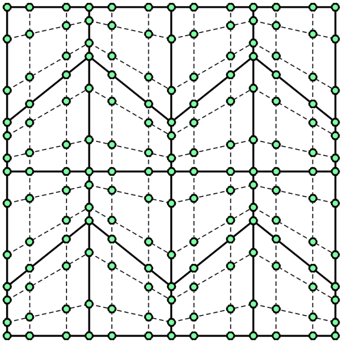

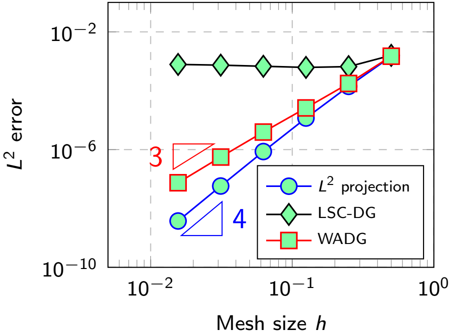

Figure: Arnold-type mesh with $\|J\|_{W^{N+1,\infty}} = O(h^{-1})$ for $N = 3$.

Behavior of weight-adjusted L^2 projection

Comparison with L^2 projection and Low-Storage Curvilinear DG

$$\tilde{\phi}_i = \frac{\phi_i}{\sqrt{J}}, \qquad \boldsymbol{M}_{ij} = \int_{D^k} \tilde{\phi}_j \tilde{\phi}_i J = \int_{\widehat{D}} \phi_j \phi_i = \widehat{\boldsymbol{M}}_{ij}.$$

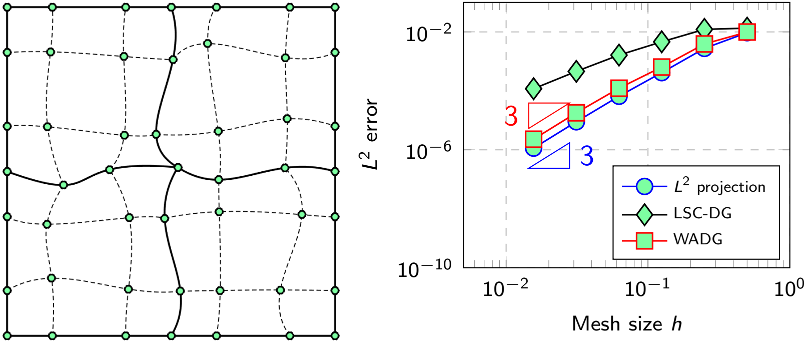

Figure: Curvilinear mesh constructed through random perturbation for $N = 3$.

Behavior of weight-adjusted L^2 projection

High order convergence slowed by growth of $\|J\|_{W^{N+1,\infty}} = O(h^N)$.

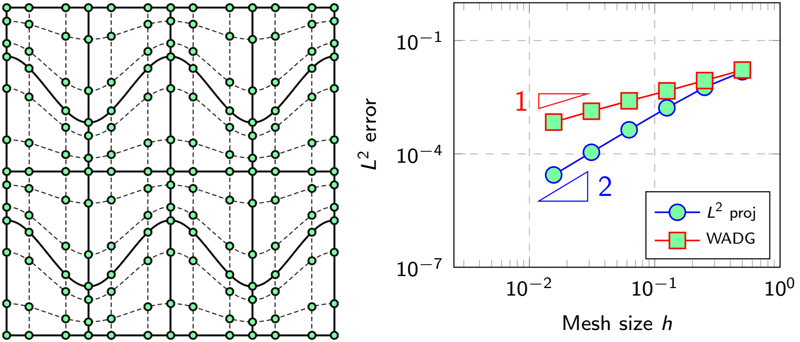

Figure: Moderately warped curved Arnold-type mesh for $N = 3$.

Behavior of weight-adjusted L^2 projection

High order convergence is stalled by growth of $\|J\|_{W^{N+1,\infty}} = O(h^{N+1})$.

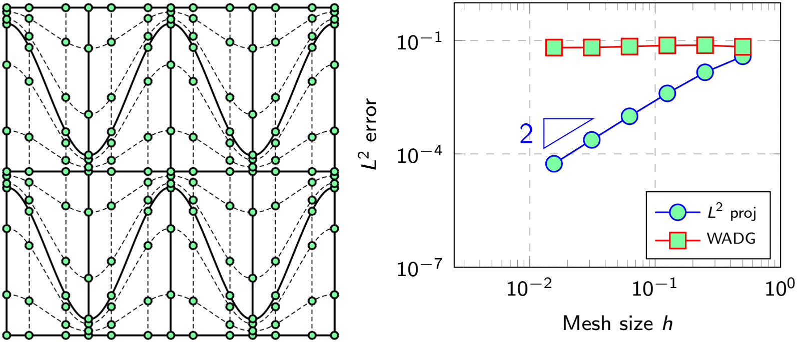

Figure: Heavily warped curved Arnold-type mesh for $N = 3$.

Weight-adjusted DG: not locally conservative

- Con: loss of local conservation for $w(x) \notin P^N$!
- Pro: superconvergence of conservation error

$$\text{Conservation error} \leq C h^{2N+2} \left\|w\right\|_{W^{N+1,\infty}} \left\|p\right\|_{W^{N+1,2}}$$

where C depends on mesh quality and max/min values of w.

- Pro: can restore local conservation with rank-1 update (Shermann-Morrison).

Effect of conservation on shock speeds

- Weighted Burgers' equation, $w(x)$ curves characteristic lines.

$$w(x)\frac{\partial u}{\partial t} + \frac{1}{2}\frac{\partial u^2}{\partial x} = 0.$$

- WADG yields high order convergence, correct shock speed for both $w(x)$ smooth, discontinuous (within an element).

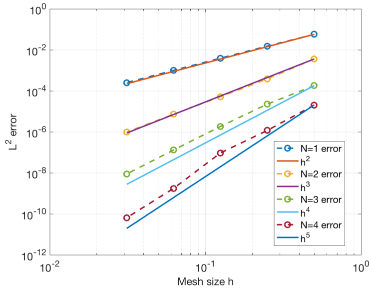

(a) Smooth solution

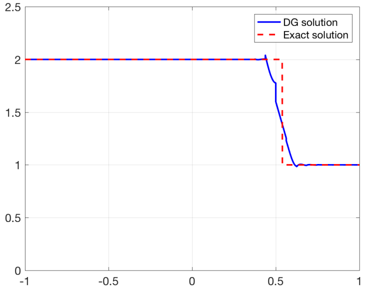

(b) Shock solution

Effect of conservation on shock speeds

- Weighted Burgers' equation, $w(x)$ curves characteristic lines.

$$w(x)\frac{\partial u}{\partial t} + \frac{1}{2}\frac{\partial u^2}{\partial x} = 0.$$

- WADG yields high order convergence, correct shock speed for both $w(x)$ smooth, discontinuous (within an element).

Best guess: where and what is locally conserved matters;
non-conservation of *nonlinear flux* results in incorrect shock speeds.